Experimental Procedures

Materials and instrumentation. All reagents and solvents were commercially available and directly used without further purification. The PXRD data were collected with a scan speed of 0.1 s·step^{-1} on a Bruker Advance D8 (40 kV, 40 mA) diffractometer with Cu radiation (λ= 1.5406 Å) at room temperature. Thermogravimetric (TGA) data were obtained on a TG 209F3 thermal analysis system with a heating rate of 10 °C min^{-1} under N2 atmosphere. Solid state cyclic voltammetry measurements were performed in n-Bu4NPF6/DMF electrolyte using a CHI 760E electrochemical work station and three electrode system. Solid-state UV-Vis-NIR spectra were obtained on the samples at room temperature using UV-3600 spectrophotometer over the wavelength range 300-1800 nm. BaSO4 was used for the baseline.

Synthesis of H4TTFTB. H4TTFTB was synthesized according to the methods of literature. [1]

Syntheses of TTFDPAT-Co-MOF, [Co^{2+}(9,10-Bis(4-pyridyl) anthracene)-H_4TTFTB^{2-}]. H_4TTFTB (13.68 mg, 0.02 mmol), $Co(NO_3)_2.6H_2O$ (11.64 mg, 0.04 mmol) and 9,10-bis(4-pyridyl) anthracene (13.28 mg, 0.04 mmol) were weighed on a weighing balance and dissolved in 3 ml of a mixture of *N*,*N*-dimethylformamide, 3 ml of ethanol and 2 ml of H_2O, and then adding 0.6 ml of acetic acid solution dropwise to dissolve. The product was filtered and washed with ethanol and dried at 60°C to obtain black lumpy crystals. The product was filtered and washed with ethanol and dried at 60°C to obtain black lumpy crystals. 13.89 mg was weighed, yield 36.00% (based on H4TTFTB).

Syntheses of TTFDPAT-Cd-MOF, [Cd^{2+}(9,10-Bis(4-pyridyl) anthracene)- H_4TTFTB^{2-}]. H_4TTFTB (6.84 mg, 0.01 mmol) was dissolved into 0.75 ml of *N*,*N*-dimethylformamide using a weighing balance, and then $Cd(ClO_4)_2$-$6H_2O$ (6.46 mg, 0.02 mmol) with 9,10-bis(4-pyridyl)anthracene (6.64 mg, 0.02 mmol) was dissolved into 1.25 ml of ethanol and 1ml of H_2O mixed solution, and the two solutions were mixed in a 10 ml glass vial and then dissolved by adding 0.2 ml of acetic acid solution dropwise. The product was filtered and washed with ethanol and dried at 60°C to obtain black flaky crystals. The product was filtered and washed with ethanol and dried at 60°C to obtain black flake crystals. 7.98 mg was obtained by weighing, yield 40.00% (based on H4TTFTB).

Near-infrared photothermal Conversion Properties Measurement. The Q-tube of 1.5 mL contained 10 mg crystal of two MOFs at the bottom and was placed at 8.0 cm from the 808 nm laser. The power density of the laser was adjusted between 0.1-2.0 W cm^{-2}. In addition, the cycle test is completed by manually turning on the 808 nm laser with a stable interval time. Infrared video of the samples was tested with an infrared thermal imaging camera (FLIR C5), and infrared photographs and real-time temperatures were extracted from the video using FLIR Thermal Studio software.

X-Ray Crystallographic Analysis

Single-crystal X-ray diffraction intensity data were collected on a Bruker APEX-II CCD diffractometer with graphite monochromatic MoKα rays (λ = 0.71073 Å) on selected single crystal samples. The CrysAlisPro-Agilent software was used to acquire data, screen diffraction points, determine lattice types and perform absorption corrections and data reduction. The structures were solved by direct methods and refined by full-matrix least-squares on *F* 2 using the SHELXTL software package.[2] Non-hydrogen atoms were refined with anisotropic displacement parameters during the final cycles. Hydrogen atoms of skeletal structure were placed at calculated ideal positions and isotropic displacement parameters were used. CCDC (TTFDPAT-Cd-MOF) 2171961 and CCDC (TTFDPAT-Co-MOF) 2211812 contain the supplementary crystallographic data for this paper. These data can be obtained free of charge from The Cambridge Crystallographic Data Centre.

Calculation of photothermal conversion efficiency.

The conversion efficiency was determined according to previous method. [3-5] Details are as follows:

$$\eta = hS\Delta T_{max} / I\,(1 - 10^{-A})$$

where I is the laser power and A808 is the absorbance of the samples at the wavelength of 808 nm.

In order to obtain the hS, a dimensionless driving force temperature, θ is introduced as follows:

$$\theta = (T - T_{surr}) / (T_{max} - T_{surr})$$

T_{max} is the maximum system temperature, and T_{surr} is the initial temperature.

$$t = -\tau s \ln \theta$$

hScould be calculated from the slope of cooling time vs ln θ.

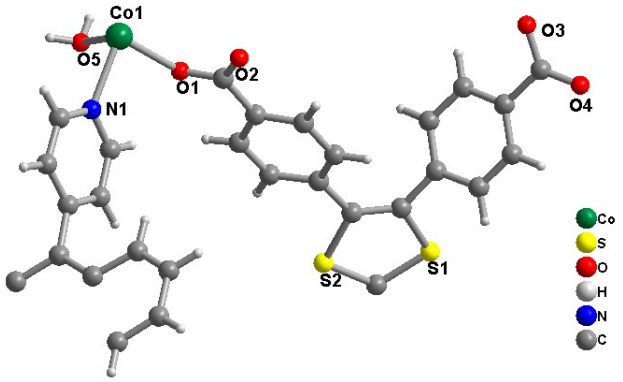

Figure S1. Asymmetric unit of **TTFDPAT-Co-MOF**.

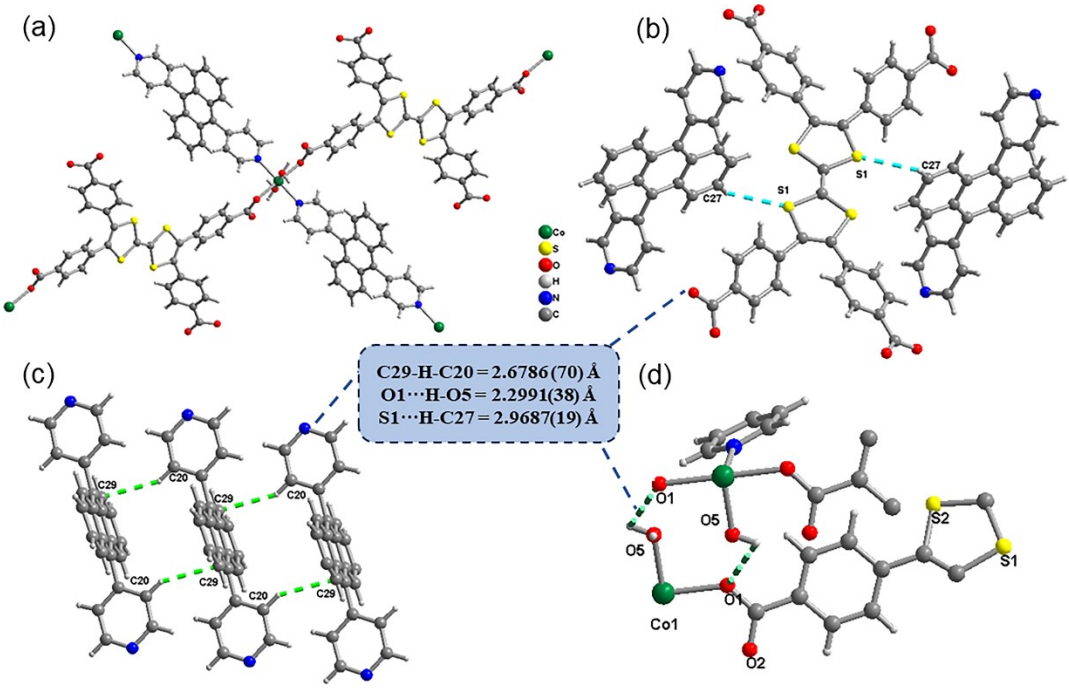

Figure S2. Coordination environments of Co (II)

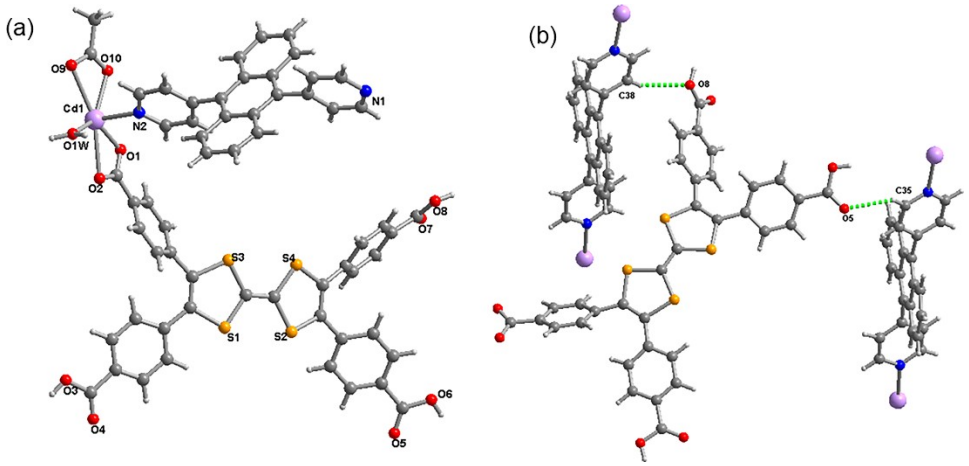

Figure S3. (a) Asymmetric unit of **TTFDPAT-Cd-MOF**. (b) Hydrogen bonding between D-A of **TTFDPAT-Cd-MOF**.

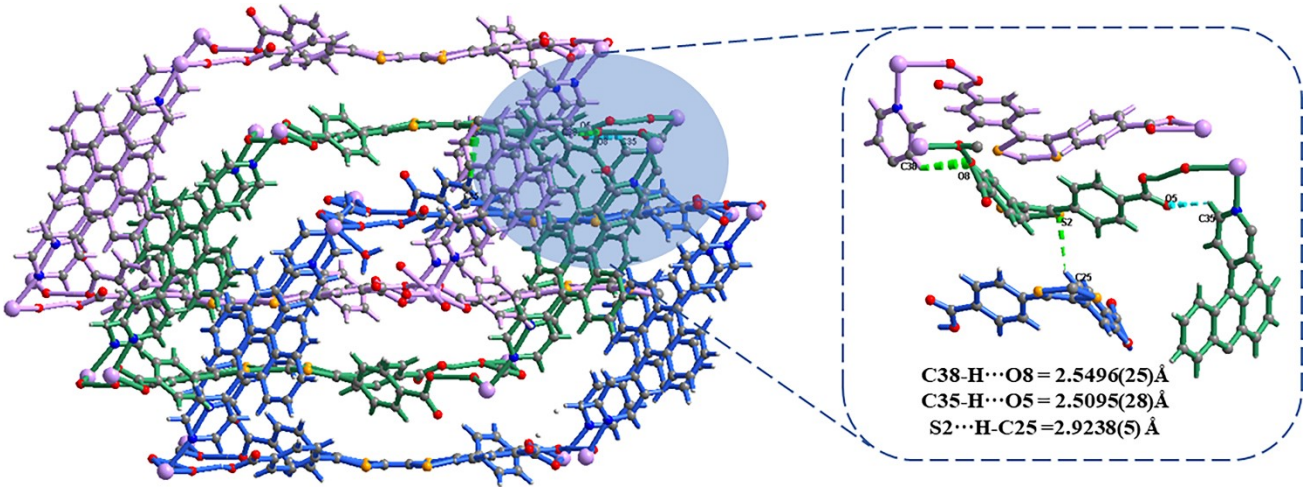

Figure S4. The distance of D and A units in the **TTFDPAT-Cd-MOF.**

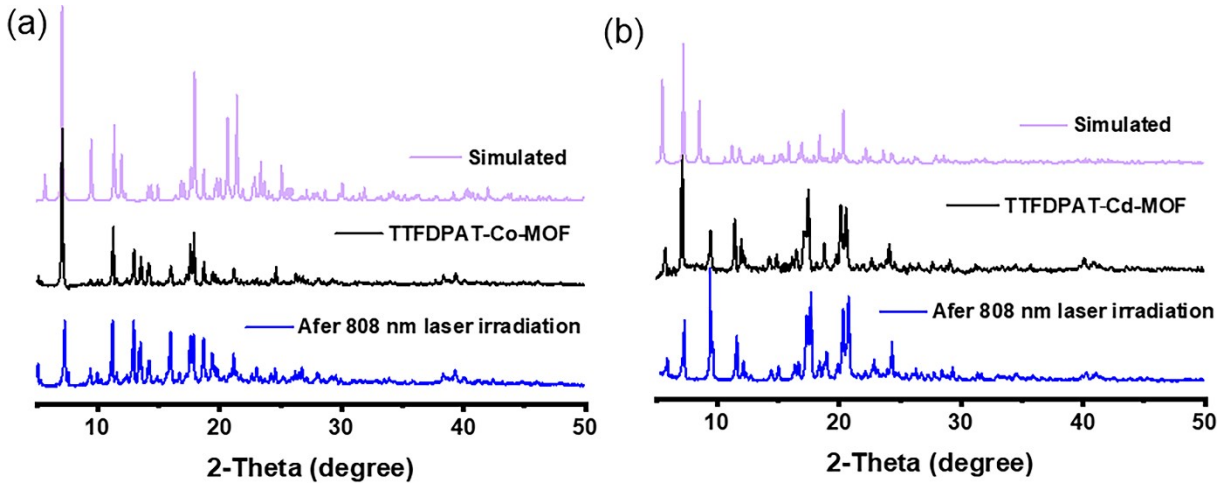

Figure S5. The powder X-ray diffraction patterns of **TTFDPAT-Co-MOF** (a) and **TTFDPAT-Cd-MOF** (b)**.**

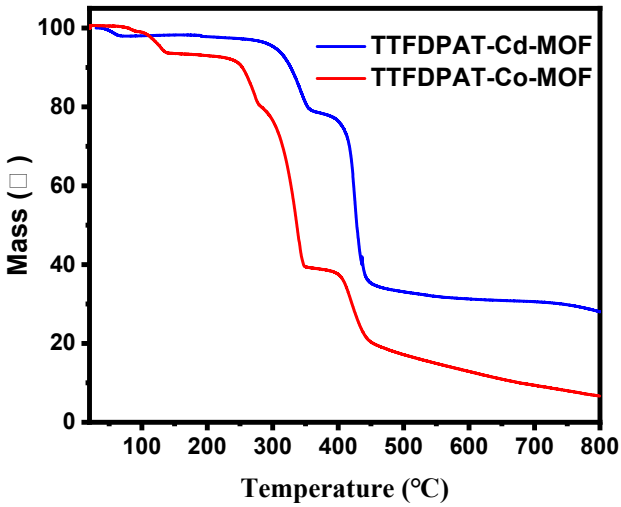

Figure S6. Thermogravimetric curves of two **MOFs**.

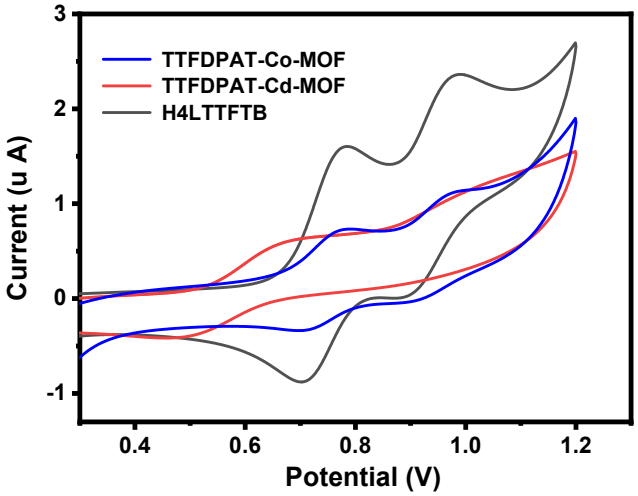

Figure S7. Solid state cyclic voltammetry curves of two MOFs.

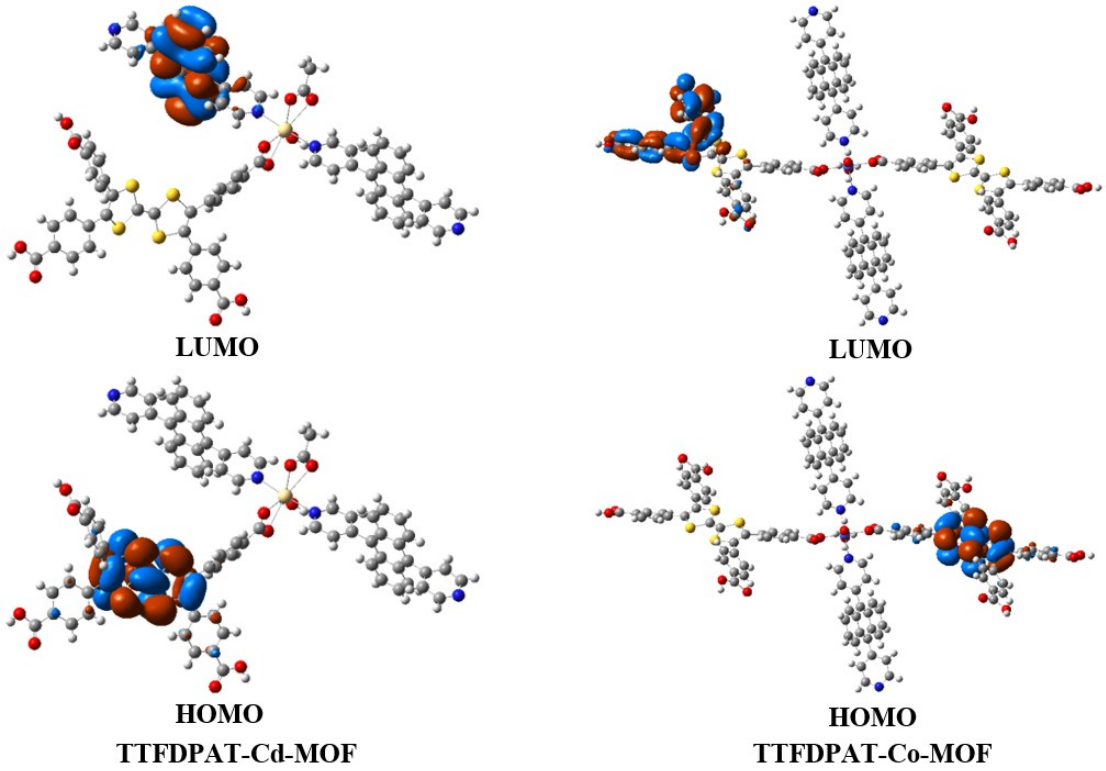

Figure S8. HOMO and LUMO electron cloud distribution pattern of asymmetric units in two MOFs.

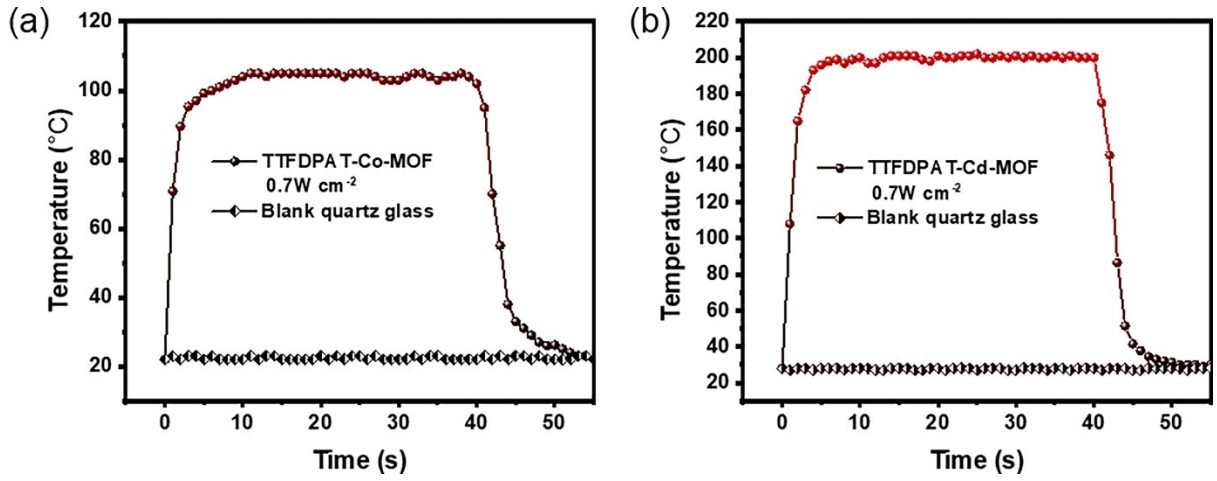

Figure S9. Photothermal conversion curves of the **TTFDPAT-Co-MOF** (a) and **TTFDPAT-Cd-MOF** (b) under 808 nm laser (0.7 W cm^{-2}) irradiation.

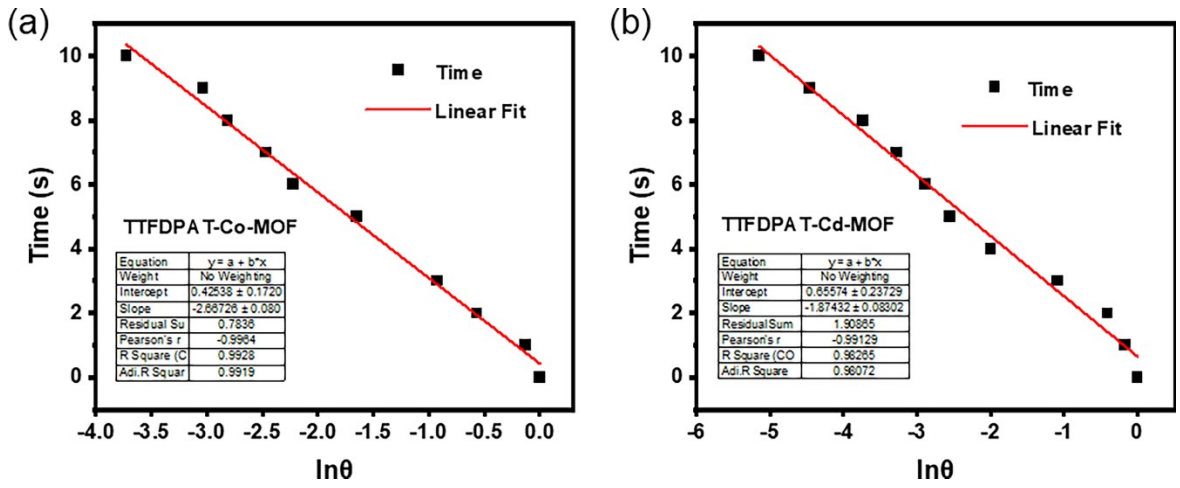

Figure S10. The time-lnθ linear curve of **TTFDPAT-Co-MOF** (a) **and TTFDPAT-Cd-MOF** (b).

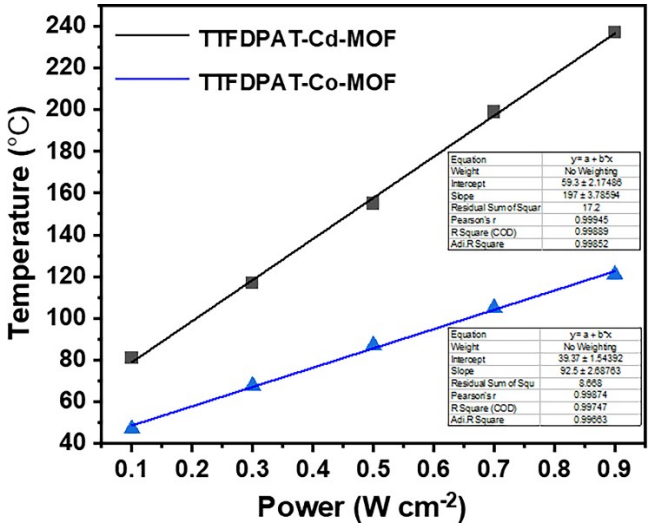

Figure S11. Plot of average temperature rise (ΔT) against power density of 808 nm laser.

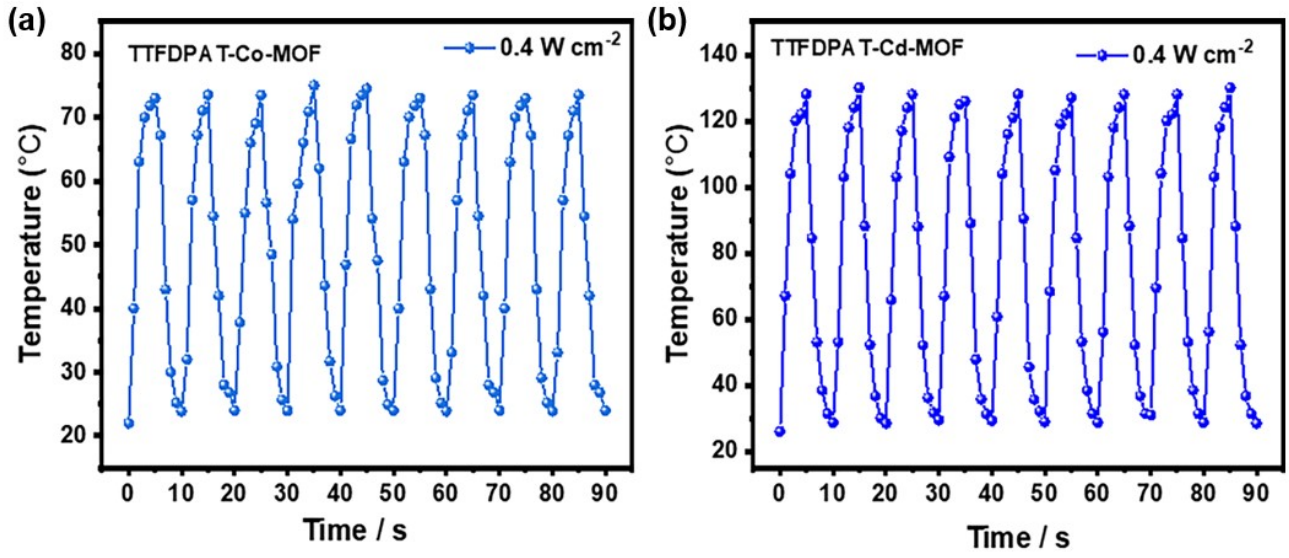

Figure S12. The Photothermal cycling test of **TTFDPAT-Co-MOF** (0.4 W cm^{-2}) (a) and **TTFDPAT-Cd-MOF** (0.4 W cm^{-2}) (b) after three weeks.

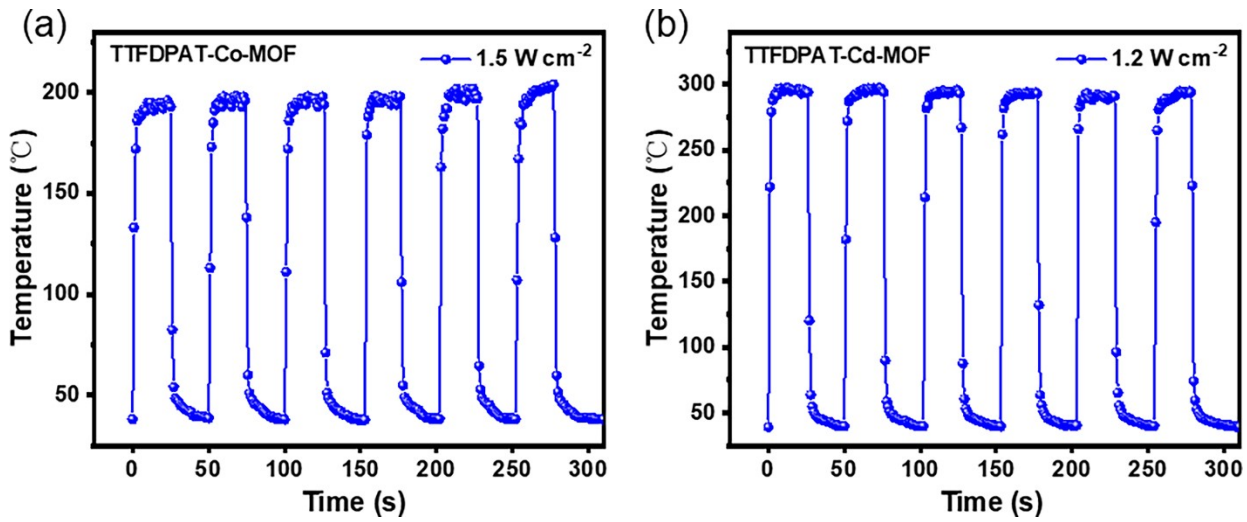

Figure S13. The Photothermal cycling test of **TTFDPAT-Co-MOF** (1.5 W cm^{-2}) (a) and **TTFDPAT-Cd-MOF** (1.2W cm^{-2}) (b).

Table S1. Crystal data and structure refinement parameters for **MOFs**

	TTFDPAT-Cd-MOF	**TTFDPAT-Co-MOF**
Empirical formula	$C_{60}H_{40}N_2O_{11}S_4Cd$	$C_{58}H_{36}CoN_2O_{10}S_4$
Formula weight	1205.58	1108.06
Temperature/K	298	298
Crystal system	triclinic	triclinic
Space group	*P-1*	*P-1*
a/Å	11.8699(7)	5.4742(16)
b/Å	15.9640(9)	15.112(4)
c/Å	16.2858(9)	16.269(4)
α/°	95.146(2)	106.279(15)
β/°	105.413(2)	92.801(16)
γ/°	103.462(2)	94.733(18)
Volume/$Å^3$	2855.2(3)	1283.8(6)
Z	2	1
ρcalcg/cm^3	1.402	1.433
μ/mm-1	0.590	0.560
F (000)	1228.0	569.0
2θ range /°	4.986 to 55.418	4.362 to 51.286
Reflections collected	97671	29387
Goodness-of-fit on F^2	1.066	1.032
R1(I＞2σ(I))	0.0363	0.0834
wR2 (all data)	0.1070	0.2392

Table S2. The NIR photothermal properties in this work compared with previous results of solid materials in the literatures

Samples	Light source	Power	Temperature ranges	Added temperature	Pretreatment	Ref
DTC co-crystal	808 nm NIR laser	0.7 W cm^{-2}	29-71.3℃	42.3℃ in 600s	None	[4]
Zr-PDI•⁻ powder	808 nm NIR laser	0.7 W cm^{-2}	25-160℃	89℃ in 100s	TEA vapor fumigation Blue light irradiation	[5]
MV-based MOF crystals	808 nm NIR laser	2 W cm^{-2}	23-110℃	88℃ in 10s	UV-visible irradiation	[6]
Tri-PMDI-TTF co-crystal	808 nm NIR laser	0.7 W cm^{-2}	15-80℃	65℃ in 200s	None	[7]
CR-TPE-T powder	808 nm NIR laser	1.2 W cm^{-2}	22-129℃	107℃ in 30s	None	[8]
Co-MOF	808 nm NIR laser	0.7 W cm^{-2}	25-201℃	99.2℃ in 5s	None	[9]
Zn-MOF	808 nm NIR laser	0.4 W cm^{-2}	25-255℃	230℃ in 24s	None	[10]
TTFDPAT-Co-MOF	808 nm NIR laser	**0.7 W cm^{-2}**	**22-105℃**	**99.2℃ in 5s**	None	**Our work**
TTFDPAT-Cd-MOF	808 nm NIR laser	**0.7 W cm^{-2}**	**25-201℃**	**196℃ in 5s**	None	

References

[1] T. C. Narayan, T. Miyakai, S. Seki and M. Dincă, *J. Am. Chem. Soc.*, 2012, ***134***, 12932-12935.

[2] G. M. Sheldrick and *Acta Crystallogr. A,* 2008, ***64***, 112-122.

[3] B. Kim, H. Shin, T. Park, H. Lim and E. Kim, *Adv. Mater*., 2013, **25**, 5483-5489.

[4] Y. Wang, W. Zhu, W. Du, X. Liu, X. Zhang, H. Dong and W. Hu, *Angew. Chem. Int. Ed.*, 2018, **57**, 3963 –3967.

[5] B. Lü, Y. Chen, P. Li, B. Wang, K. Müllen and M. Yin, *Nat. Commun.*, 2019, **10**, 767.

[6] S. Wang, S. Li, J. Xiong, Z. Lin, W. Wei and Y. Xu, *Chem. Commun.,* 2020, **56**, 7399-7402.

[7] D. Wang, X. Kan, C. Wu, Y. Gong, G. Guo, T. Liang, L. Wang, Z. Li and Y. Zhao, *Chem. Commun.,* 2020, ***56***, 5223-5226.

[8] G. Chen, J. Sun, Q. Peng, Q. Sun, G. Wang, Y. Cai, X. Gu, Z. Shuai and B. Z. Tang, *Adv. Mater.*, 2020, ***32***, e1908537.

[9] T. Yan, Y. Y. Li, J. Su, H. Y. Wang and J. L. Zuo, *Chem. Eur. J.*, 2021,**27**,11050-11055.

[10] T. Yan, Y. Y. Li, Q. Y. Gu, J. Li, J. Su, H. Y. Wang and J. L. Zuo, *Inorg. Chem.*, 2022, **61**, 3078−3085.